



# Chemical and semiconducting properties of NO<sub>2</sub>-activated H-terminated diamond

M.W. Geis<sup>a,\*</sup>, T.H. Fedynyshyn<sup>a,\*</sup>, M.E. Plaut<sup>a</sup>, T.C. Wade<sup>a,\*</sup>, C.H. Wuorio<sup>a</sup>, S.A. Vitale<sup>a</sup>,  
J.O. Varghese<sup>a</sup>, T.A. Grotjohn<sup>b</sup>, R.J. Nemanich<sup>c</sup>, M.A. Hollis<sup>a</sup>

<sup>a</sup> Lincoln Laboratory, Massachusetts Institute of Technology, Lexington, MA, United States

<sup>b</sup> Electrical and Computer Engineering, Michigan State University, East Lansing, MI, United States

<sup>c</sup> Physics, Arizona State University, Tempe, AZ, United States

## ARTICLE INFO

### Keywords:

Diamond  
Hydrogen-termination  
Molecular adsorption  
Nitrogen dioxide

## ABSTRACT

The H-terminated surface of diamond when activated with NO<sub>2</sub> produces a surface conduction layer that has been used to make field effect transistors (FETs). Previous reports have suggested that during NO<sub>2</sub> exposure (NO<sub>2</sub>-activation), NO<sub>2</sub><sup>-</sup> forms on the diamond surface and generates positive carriers (holes) in the diamond, making the diamond surface conductive. We report here on X-ray-photoelectron-spectroscopy (XPS) surface characterization of single crystal diamonds and on infrared absorption of diamond powder. After activation, XPS showed the presence of N atoms on the diamond surface, but infrared absorption found no evidence of NO<sub>2</sub><sup>-</sup>, but instead NO<sub>3</sub><sup>-</sup> is present on the diamond surface.

Two wet chemistry techniques determined the concentration of NO<sub>3</sub><sup>-</sup> per milligram of diamond powder. With the powder's surface area measured by the BET technique, the surface NO<sub>3</sub><sup>-</sup> concentration was measured to be between  $6.2 \times 10^{13}$  and  $8.2 \times 10^{13}$  cm<sup>-2</sup>. This is in the same range as the carrier densities,  $3 \times 10^{13}$  to  $9 \times 10^{13}$  cm<sup>-2</sup>, determined by Hall mobility and surface conductivity measurements of single crystal diamonds. Using similar techniques, the concentration of NO<sub>2</sub><sup>-</sup> was determined to be  $< 10^{12}$  cm<sup>-2</sup>.

Both the surface conductance and the surface H atoms are stable in dry nitrogen, with or without NO<sub>2</sub>-activation, but the surface conductance, the concentrations of H atoms both with and without activation and NO<sub>3</sub><sup>-</sup> decrease when exposed to laboratory air over a period of hours to days. Infrared absorption measurements showed the reduction of surface NO<sub>3</sub><sup>-</sup> and H atoms during laboratory air exposure, but gave no indication of what reactions are responsible for their loss in laboratory air.

## 1. Introduction

When the surface of diamond is covered with H atoms (H-terminated) the diamond becomes conductive when exposed to air [1]. This conductivity is further enhanced when covered with a layer of a high-work-function material (activation) by transfer doping [2,3]. Impressive field effect transistors (FETs) have been made, using this conductive layer with current densities  $> 1$  A/mm [4,5], a wide operational temperature range,  $-263$  (10 K) to  $400$  °C [4], high-voltage operation  $> 1$  kV [4,6], and high maximum frequency of oscillation,  $f_{\text{max}}$ ,  $\sim 100$  GHz [7,8]. Of all the high-work-function activation compounds, MoO<sub>3</sub> [9,10], V<sub>2</sub>O<sub>3</sub> [9,11] Al<sub>2</sub>O<sub>3</sub> [4], and others, the gas, NO<sub>2</sub>, gives one of the lowest surface resistances  $\sim 700$  Ω sq<sup>-1</sup> [12]. However, during FET fabrication, the surface resistance increases by nearly an order of magnitude to  $\sim 5$  kΩ sq<sup>-1</sup>. Still, to date NO<sub>2</sub>-activated diamond FETs exhibit the highest drain current  $\sim 1.3$  A/mm [5,8]. This

article discusses the chemistry of NO<sub>2</sub>-diamond activation and how it impacts the surface conductance.

NO<sub>2</sub> was first identified as being capable of activating diamond at concentrations as low as 5 to 10 parts per billion (ppb) [13,14]. Natural concentrations of NO<sub>2</sub> in air is from 20 to 60 ppb [15], and along with other atmospheric components cause the H-terminated diamond surface to become conductive over tens of minutes. Unsurprisingly, atmospheric activation is inconsistent and unstable in time as other atmospheric components (NH<sub>3</sub>, organic amines etc.) will deactivate diamond or irreversibly react with the diamond surface, increasing the surface resistance to  $> 10$  kΩ sq<sup>-1</sup>. Kasu et al. suggested two mechanisms for NO<sub>2</sub>-activation. In the first mechanism, NO<sub>2</sub> pulls electrons out of the diamond to form the conductive hole layer and NO<sub>2</sub><sup>-</sup> [16,17]. In the second mechanism, some unknown reaction occurs on the diamond surface, forming a negative surface charge, not NO<sub>2</sub><sup>-</sup>, and hole conduction in the diamond [18]. We favor the latter of the two models.

\* Corresponding authors.

E-mail addresses: [Geis@LL.mit.edu](mailto:Geis@LL.mit.edu) (M.W. Geis), [Fedynyshyn@LL.mit.edu](mailto:Fedynyshyn@LL.mit.edu) (T.H. Fedynyshyn), [Travis.Wade@LL.mit.edu](mailto:Travis.Wade@LL.mit.edu) (T.C. Wade).

<https://doi.org/10.1016/j.diamond.2018.03.002>

Received 12 January 2018; Received in revised form 28 February 2018; Accepted 5 March 2018

Available online 06 March 2018

0925-9635/ © 2018 Elsevier B.V. All rights reserved.

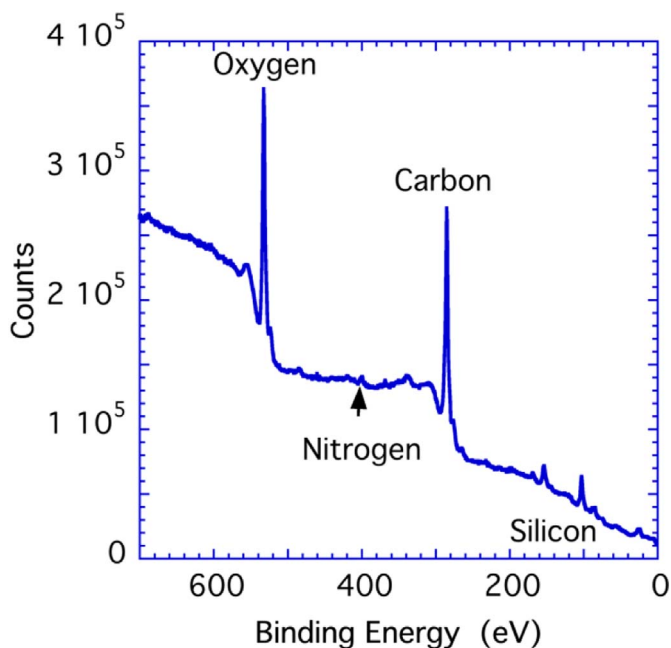


Fig. 1. X-ray photoelectron spectroscopy (XPS) of a single crystal (100) H-terminated  $\text{NO}_2$ -activated diamond. The electron intensity peaks are labeled with their corresponding elements. The silicon peak is believed from impurities incorporated into the diamond during growth.

Using x-ray-photoelectron-spectroscopy (XPS), Fourier-transform-infrared-spectroscopy (FTIR), wet chemical analysis for  $\text{NO}_2^-$  and  $\text{NO}_3^-$ , and electrospray mass spectrometry (ESMS), we found no evidence of  $\text{NO}_2^-$ , but instead found concentrations of  $\text{NO}_3^-$  matching the surface hole concentrations,  $3 \times 10^{13}$  to  $9 \times 10^{13} \text{ cm}^{-2}$  as calculated from Hall mobility and surface conductivity. Additionally, the  $\text{NO}_2$  reacts with the hydrogen atoms on the H-terminated diamond surface, removing between 25 and 75% of them. While it is believed that the presence of  $\text{NO}_3^-$  is a necessary condition for diamond hole conduction, it is unknown what impact the removal of H atoms has on the conduction or what replaces it in the areas where hydrogen is removed.

## 2. Experimental procedure and characterization

Several characterization tools have been applied to characterize the effect of  $\text{NO}_2$  on H-terminated diamond.

### 2.1. XPS

XPS of H-terminated,  $\text{NO}_2$ -activated (100) diamond is shown in Figs. 1 and 2. The diamond was etched in molten  $\text{NaNO}_3$ , H-terminated and  $\text{NO}_2$  activated as described by Wade et al. [19]. These results are similar to those of Kasu [18] with O and C atoms covering most of the surface, but no indication of N atoms. However, on closer examination of our diamond there is a weak N signal, Fig. 2. From the ratio of the areas, using a Mg anode target and the sensitivity factors for the Perkin Elmer model 5500, the concentrations of C:O:N respectively,  $M_i$ , were 68.6%, 29.7% and 1.7%. Neglecting the O concentration and assuming all the N atoms are on the diamond surface, the concentration of N atoms in monolayers,  $\Theta_N$ , is estimated by [20].

$$\Theta_N = \frac{M_N}{M_C} \times \sum_{n=0}^{\infty} \exp\left[\frac{-n*d_{Dia}}{\lambda_{Dia}*\cos(\varphi)}\right]$$

$$= \frac{M_N}{M_C} \left[1 - \exp\left[\frac{-d_{Dia}}{\lambda_{Dia}*\cos(\varphi)}\right]\right]^{-1}$$

$M_N$  and  $M_C$  are the concentrations of N and C atoms;  $d_{Dia}$  is the

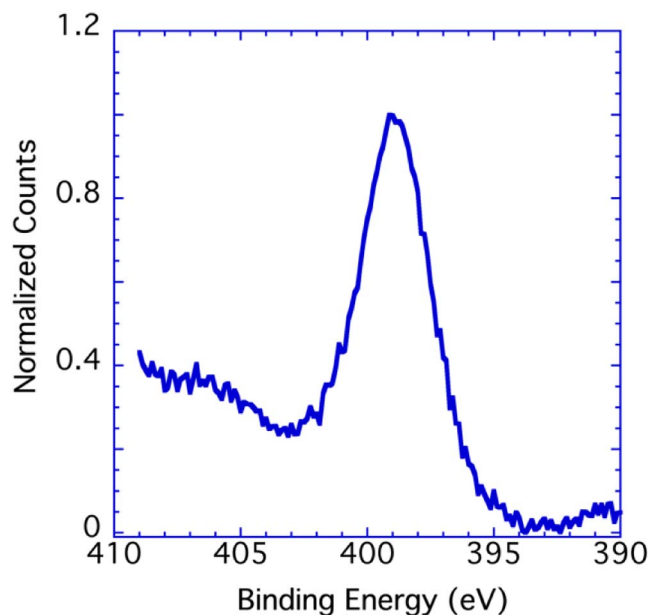


Fig. 2. XPS over the binding energies assigned to nitrogen. The integrated area under the peak associated with N is 1.7% of the combined areas of O, N and C. Carbon area is 68.6% and O is 29.7%.

spacing between two (100) planes, 0.357 nm; take off angle,  $\varphi$ , is  $45^\circ$ ; and  $\lambda_{Dia}$  is the electron attenuation length, EAL, of C1s electrons,  $\sim 1.74 \text{ nm}$  at an electron energy of  $\sim 970 \text{ eV}$  [21]. The estimated N coverage is 0.098 monolayer or  $1.5 \times 10^{14} \text{ cm}^{-2}$ .

After XPS characterization, the sample's resistance was  $7 \text{ k}\Omega \text{ sq}^{-1}$  with a Hall mobility of  $30 \text{ cm}^2 \text{ V}^{-1} \text{ s}^{-1}$  giving an estimated carrier density of  $3.0 \times 10^{13} \text{ cm}^{-2}$ . Assuming each N atom represents a negatively charged molecule that generates a hole, the XPS-estimated N surface density is within an order of magnitude of the carrier density. The peak associated with O is likely from absorbed  $\text{H}_2\text{O}$  and  $\text{CO}_2$  and chemically bounded OH and CO. All of which appear in the infrared spectrum discussed below. Although,  $\text{H}_2\text{O}$  and  $\text{CO}_2$  individually have been shown not to contribute to surface conduction [8], they may increase conductance in combination with other components.

The XPS measured binding energies are 283.9 eV for C and 399.1 eV for N. The binding energy for C is consistent with a H-terminated diamond surface [22]. However, the binding energy for N is consistent with cyanides, CN, and not for the binding energies of nitrites,  $\text{NO}_2^-$ , 404–405 eV or nitrates,  $\text{NO}_3^-$ , 407–408 eV [23]. Since we see only N in the form of nitrates as discussed below using FTIR, we speculated that XPS emission from nitrates is shifted by a negative potential locally on the surface where the nitrates are absorbed compared to the bulk of the diamond.

### 2.2. Infrared absorption by FTIR

XPS is a powerful technique, but does not have the ability to accurately determine surface concentrations and molecular structure at low surface concentration levels,  $1 \times 10^{12} \text{ cm}^{-2}$ . Another approach, infrared absorption with FTIR of diamond powder was used. It has sensitivity to surface concentrations of  $< 1 \times 10^{12} \text{ cm}^{-2}$  depending upon the diamond powder's surface area per gram and the infrared optical cross section of the surface component. Diamond powder, 0 to 0.25, formed from high-pressure high-temperature (HPHT) diamonds, washed with 1 to 1 HCl and  $\text{H}_2\text{O}_2$ , heated to  $525^\circ \text{C}$  in air for  $> 15 \text{ h}$ , and stored in dry  $\text{N}_2$ , was used as the starting material. Figs. 3 and 4 show a wide distribution in particle size. H-termination was accomplished by first evenly dispersing 60 to 100 mg of powder in a 2.5 cm circle centered on a  $2.25 \times 2.25 \times 0.025$ -inch  $\text{Al}_2\text{O}_3$  plate. H-

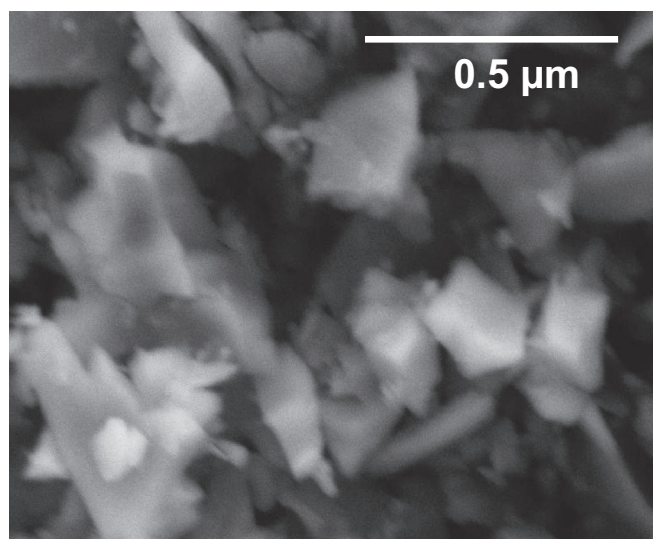


Fig. 3. Scanning electron micrograph, SEM, of a thick layer of diamond powder on a Si wafer.

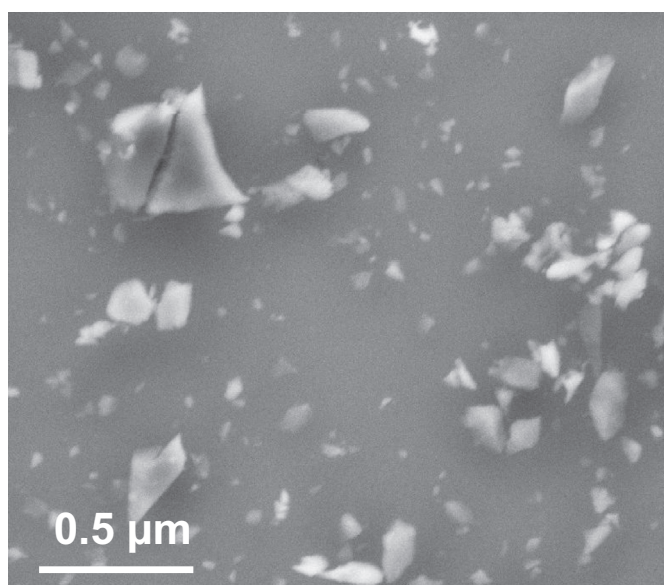


Fig. 4. SEM of diamond powder dispersed on a Si wafer showing a large range in particle sizes.

termination in a 100%-H<sub>2</sub> 6 -kW plasma [19] proceeded by first degassing the powder at 90 Torr (12 kPa) of H<sub>2</sub> to generate a diamond powder surface temperature > 1000 °C for 10 min, as shown in Figs. 5 and 6. This is followed by a 1 h H-termination process at 60 Torr (8 kPa) of H<sub>2</sub>. The chamber pressure reduction expands the plasma, reduces both the heat flux, and the temperature from > 1000 °C to between 820 and 870 °C. After H-termination, the power's surface temperature is gradually reduced such that the plasma is still present when the surface temperature is < 400 °C. The powder was then exposed to NO<sub>2</sub> at room temperature and pressure for 20 min. The NO<sub>2</sub> was generated from concentrated HNO<sub>3</sub> reacting with copper turnings. A video walk-through of NO<sub>2</sub> activation is shown in reference 19. The activated powder was then placed in a chamber of flowing dry N<sub>2</sub> for at least 10 min to remove excess NO<sub>2</sub> vapor and minimize any condensation of water. Then 1 or 4 mg of the powder was removed for FTIR measurements.

FTIR was performed by using a common procedure [24] of mixing either 1 or 4 mg of diamond powder with 50 mg of infrared transparent potassium bromide, KBr. The mixture was then pressed to form a pellet

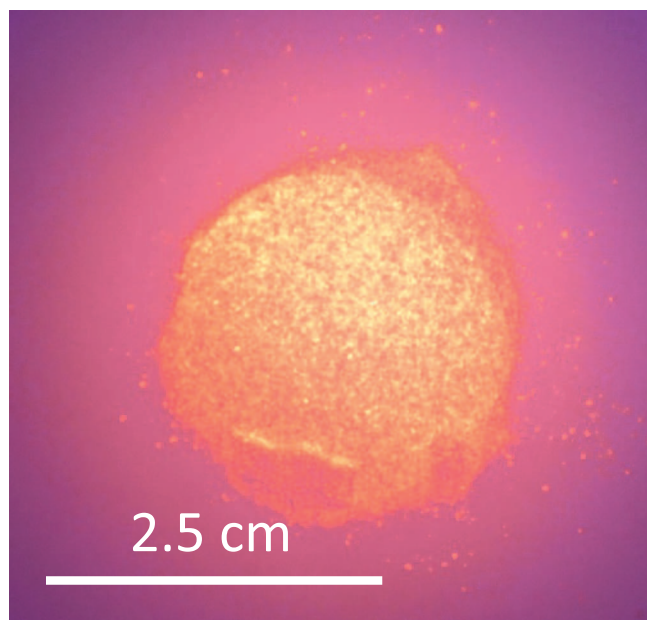


Fig. 5. Top-down image of diamond powder during H-termination.

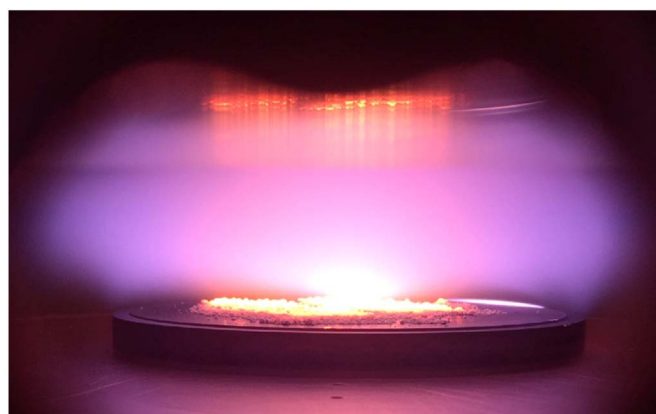


Fig. 6. Side view of diamond powder during H-termination. The powder has a surface temperature of ~1000 °C. Temperature was determined by an optical pyrometer taking the ratio of light intensities at 2.2 and 2.4 μm.

and infrared absorption of the pellet was measured using FTIR. Special precautions are required when using powdered diamond to obtain usable pellets as described in the supplemental material. Fig. 7 shows a typical FTIR spectrum with the majority of the measured absorption due to scattering of light by the powder and not by actual infrared absorption. Light scattering losses can be compensated for by fitting the absorption to a smooth curve and subtracting it from the measured absorption. For the data shown here the compensation was accomplished by a commercial baseline correction software [25], using the “rubber band” procedure as shown in Figs. 7 and 8.

Fig. 8 shows the resulting absorption data as the smooth curve is iterated with a higher degree of compliance to the measured absorption and thus removing other scattering artifacts, but it can also remove the actual infrared absorption peaks. Iterations > 50 can remove broad ill-defined absorption peaks entirely [25]. Adsorbed H<sub>2</sub>O, which has a wide optical absorption from 3600 to 3100 cm<sup>-1</sup> [26,27], is such a peak. FTIR reduced data shown here have 17 iterations unless otherwise stated. Fig. 9 shows FTIR spectra of starting and H-terminated diamond powder. The absorptions for O–H, C–H and C=O are assigned to be stretching vibrations at or near 3780, 2928–2840 and 1765 cm<sup>-1</sup> respectively and we tentatively assign the absorption peaks

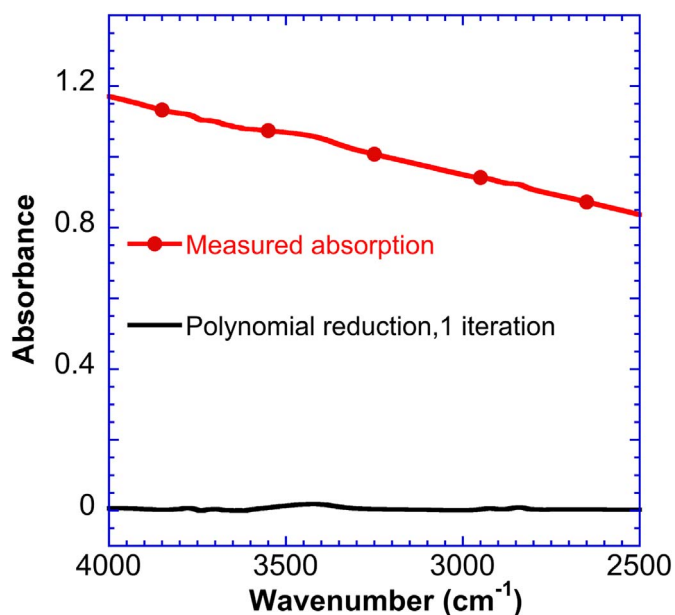


Fig. 7. Typical FTIR absorption of a diamond-powder KBr pellet in red and the first “rubber band” correction iteration in black. (For interpretation of the references to color in this figure legend, the reader is referred to the web version of this article.)

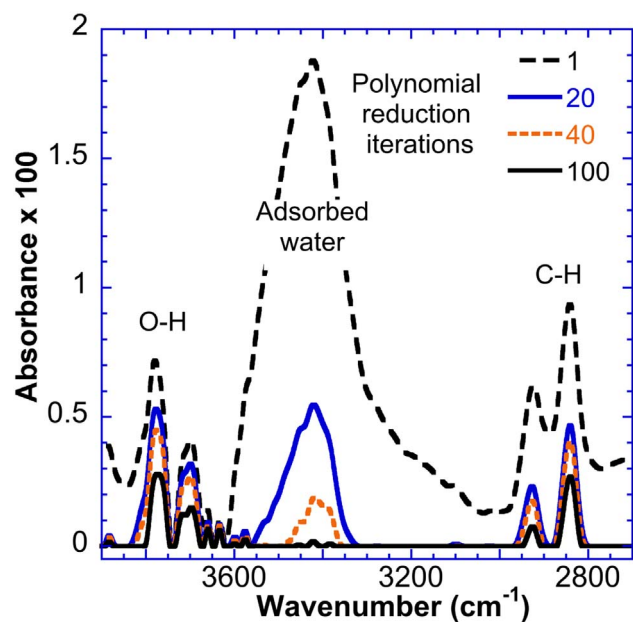


Fig. 8. First “rubber band” correction iteration from Fig. 7 in dashed black and resulting reduced absorption curves with further iterations. Some of the absorption peaks are labeled with the molecules responsible for the infrared absorption.

at 770 and 726  $\text{cm}^{-1}$  to C–H bending vibrations. The absorption near 2400  $\text{cm}^{-1}$  is an artifact from atmospheric  $\text{CO}_2$  and not from the sample. Upon H-termination the O–H at 3780  $\text{cm}^{-1}$  is gone and C–H absorption is dominant, showing that the diamond surface is indeed H-terminated. A higher resolution spectrum of the C–H stretching vibration absorption is shown in Fig. 10. Also shown are wavenumber assignments of H-terminated diamond from the literature with crystal planes, hydrogen-carbon bonding structures (C–H or C–H<sub>2</sub>), wavenumbers, and references. Some controversy still exists on how H is bonded to the diamond surface [33], which is not addressed in this article.

Upon hydrogen termination, the surface is initially highly resistive ( $> 20 \text{ M}\Omega \text{sq}^{-1}$ ), shifting to 10–20  $\text{k}\Omega \text{sq}^{-1}$  over tens of minutes in

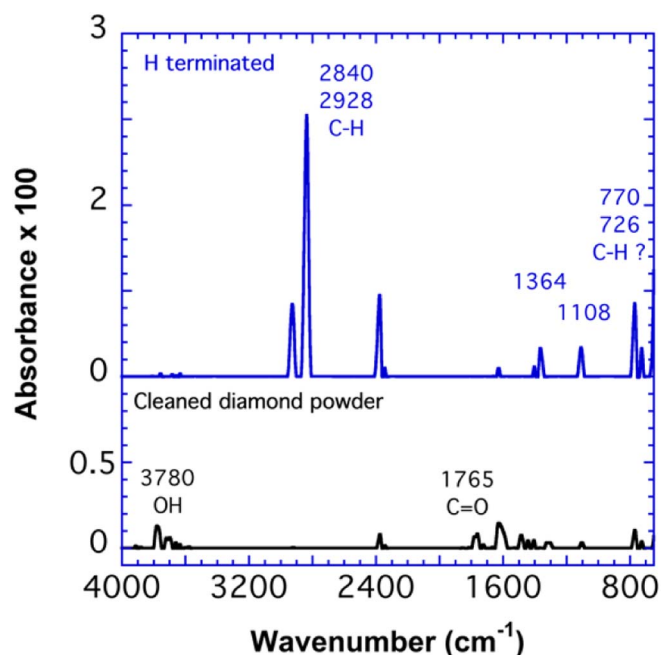


Fig. 9. Absorption spectrum of starting and H-terminated diamond powder. The data has 100 iterations of the baseline correction to emphasize the O–H and C–H spectrum. This minimizes the broad absorption peak of adsorbed water.

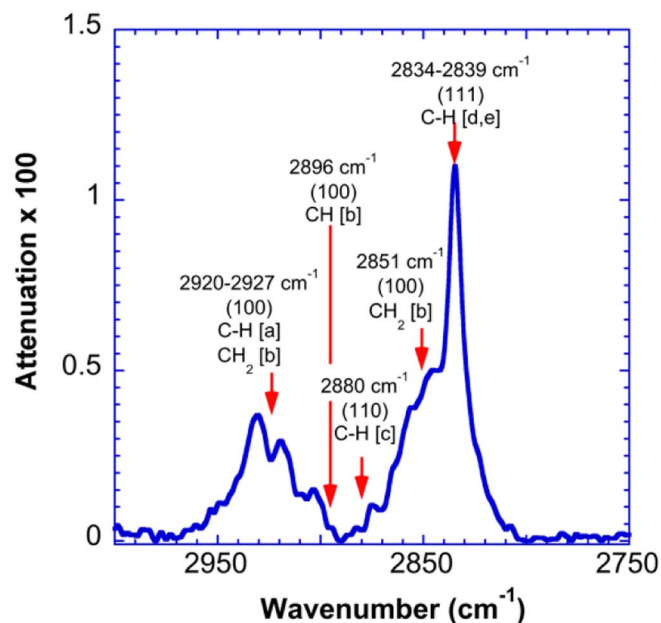


Fig. 10. A high-resolution,  $2 \text{ cm}^{-1}$ , of C–H absorption spectrum, of H-terminated diamond powder with 17 iterations of the baseline correction. From the literature, crystal planes, atomic structures responsible for the absorption, wavenumbers, and references are shown. [a] Ref [28], [b] Ref [29], [c] Ref [30], [d] Ref [31], and [e] Ref [32].

laboratory air. The exact magnitude of the resistance is observed to be dependent on uncontrolled atmospheric factors. In particular, we have correlated resistivity variations of 7–10  $\text{k}\Omega \text{sq}^{-1}$  with air handler cycling.

H-termination by  $\text{H}_2$  plasma is sensitive to low concentrations of  $\text{CH}_4$  and  $\text{O}_2$ . The addition of 0.25% of  $\text{CH}_4$  to the  $\text{H}_2$  during termination reduces the C–H concentration as measured by FTIR by half and roughly triples the surface resistance on single crystal diamonds [19]. Oxygen can both increase or decrease C–H concentration depending on the presence of a carbon source in the plasma chamber. To improve

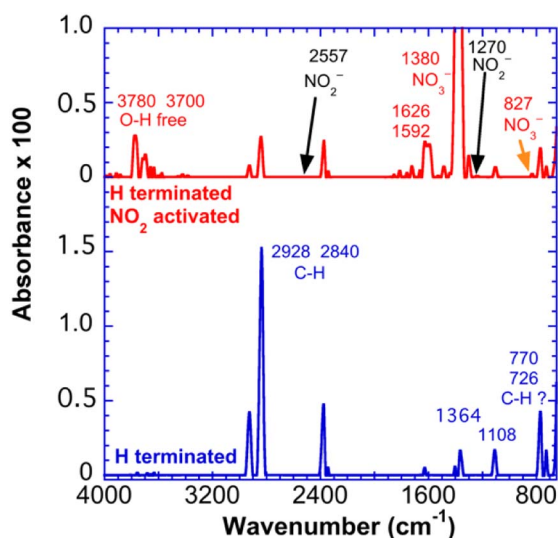


Fig. 11. Absorption spectrum of diamond powders, for H-terminated and H-terminated and  $\text{NO}_2$ -activated. The data has 100 iterations of the baseline correction to emphasize the O–H, C–H, and  $\text{NO}_3^-$  spectrum. No absorption for  $\text{NO}_2^-$  is observed at its assigned wavenumbers, 1270 and  $2557\text{ cm}^{-1}$  [36,37].

reproducibility, the microwave plasma diamond deposition system is cleaned with a  $\text{H}_2\text{-O}_2$  plasma for an hour to remove carbon deposits from chamber walls and substrate fixturing that can form during the epitaxial growth prior to H-termination.

The effect of  $\text{NO}_2$ -activation on H-terminated powder is shown in Fig. 11, comparing H-terminated powder before and after activation. The C–H vibration is significantly reduced and absorption at  $1380\text{ cm}^{-1}$ , which we assign to  $\text{NO}_3^-$  [34,35] appears. Arrows in the figure show where  $\text{NO}_2^-$  would appear [36,37] if it were present. Although many such spectra have been acquired, no indication of  $\text{NO}_2$  or  $\text{NO}_2^-$  has ever been found. Upon  $\text{NO}_2$ -activation a sudden and large reduction of resistance occurs. However, others have reported afterwards even in  $\text{N}_2$  the resistivity increases and the charge carrier density decreases in some cases by  $\sim 50\%$  in 5 h. This is attributed to  $\text{NO}_2^-$  losing its electron to the diamond and evaporating as a gas [14,38]. Reported here the FTIR data shows that  $\text{NO}_3^-$  (Fig. 12) and C–H concentrations in dry  $\text{N}_2$  remaining constant for 75 h, > 3 days. The

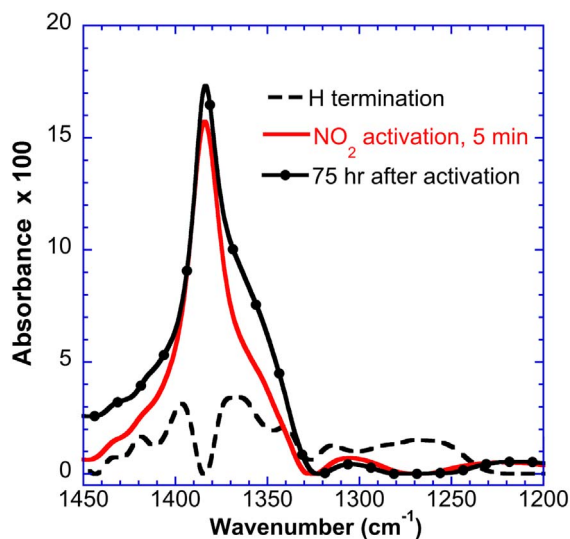


Fig. 12. Absorption spectrum of diamond powders for H-terminated, H terminated and  $\text{NO}_2$ -activated, and H-terminated and  $\text{NO}_2$ -activated after > 3 days dry in  $\text{N}_2$ , all with 17 iterations of the baseline correction. The absorption peak at  $1380\text{ cm}^{-1}$  is assigned to  $\text{NO}_3^-$ .

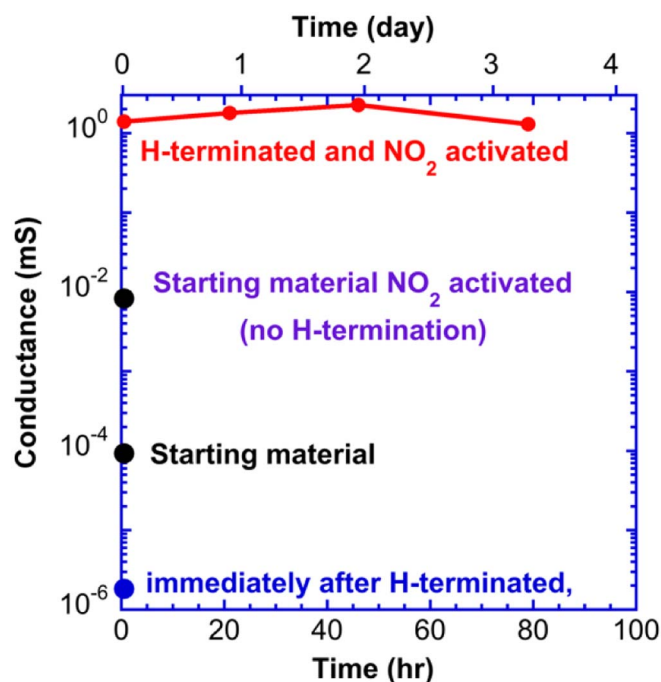


Fig. 13. Conductance of H-terminated  $\text{NO}_2$ -activated diamond powder as a function of time in dry  $\text{N}_2$ . The resistance of starting (no H-termination),  $\text{NO}_2$ -activated starting, and H-terminated diamond powder are also shown for comparison.

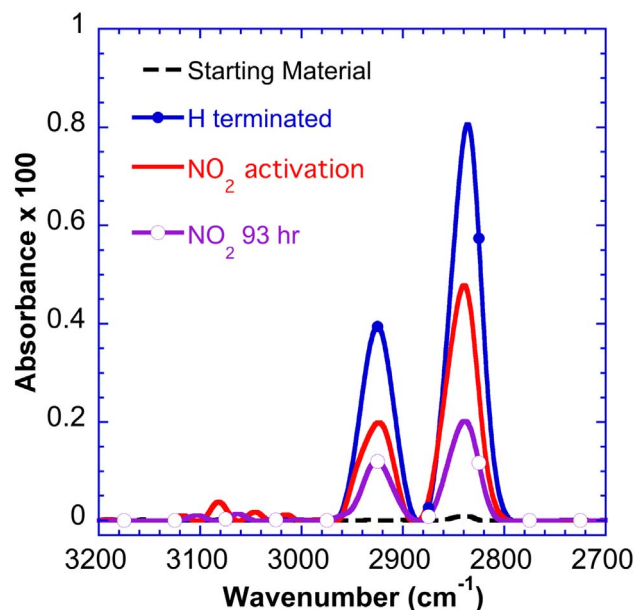


Fig. 14. C–H absorption spectra of diamond. H-terminated and H-terminated and  $\text{NO}_2$ -activated for several times after activation, all with 17 iterations of the baseline correction. The powder was exposed to laboratory air after activation.

resistivity of the same powder is also constant over the same period (Fig. 13). If the powder is exposed to laboratory air, both the  $\text{NO}_3^-$  and C–H concentrations decrease in time, as shown by Figs. 14 and 15. We found the resistance of single-crystal H-terminated  $\text{NO}_2$ -activated diamonds is stable in dry  $\text{N}_2$  for days but increases in laboratory air [19].

The infrared signature of C–H decreases with  $\text{NO}_2$ -activation as shown at higher resolution in Fig. 16. Previous experiments, not reported here, show the C–H absorption peaks at 2850 and 2950 can vary independently, indicating that the peaks are from different crystal planes or different C–H structures. To within the experimental accuracy,  $\text{NO}_2$ -activation appears to affect both absorptions regions equally.

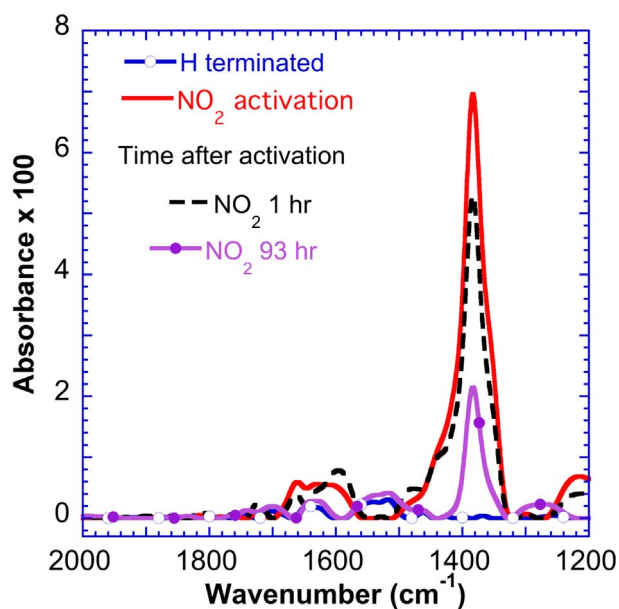


Fig. 15.  $\text{NO}_3^-$  absorption spectra of diamond powder H-terminated and  $\text{NO}_2$ -activated for several times after activation all with 17 iterations of the baseline correction. The powder was exposed to laboratory air after activation.

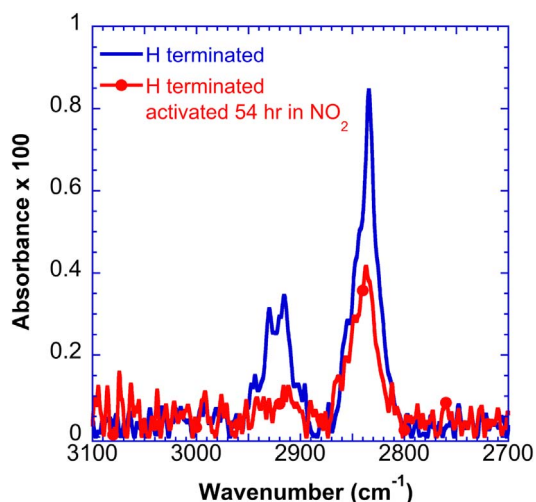


Fig. 16. High resolution,  $2\text{ cm}^{-1}$ , C–H absorption spectra of diamond powder H-terminated and after an extended activation, 54 h in  $\text{NO}_2$  both with 17 iterations of the baseline correction.

While the C–H absorption continues to decrease after activation in laboratory air, Figs. 14, 17 and its insert show that C–H absorption and surface conductance of single crystal diamond with no activation also decreases in air. When controlling the ambient environment (dry  $\text{N}_2$ ) hydrogen termination is stable over extended periods, measured over weeks and anecdotally observed over years. Since the  $\text{O}_2$ ,  $\text{N}_2$ , and  $\text{H}_2\text{O}$ , the major components of air, are expected to be unreactive, some other trace component is probably responsible.

### 2.3. Absolute measurement of $\text{NO}_3^-$ and $\text{NO}_2^-$

To estimate the surface concentration of  $\text{NO}_3^-$  on H-terminated powder surface after activation, two measurements were performed. The concentrations of  $\text{NO}_3^-$  and  $\text{NO}_2^-$  per mg of activated powder were determined by wet chemical analysis [39] and electrospray mass spectrometry (ESMS) [40]. The H-terminated powders were activated and 60 to 100 mg of the powders were washed in 1.5 ml of 0.1 M

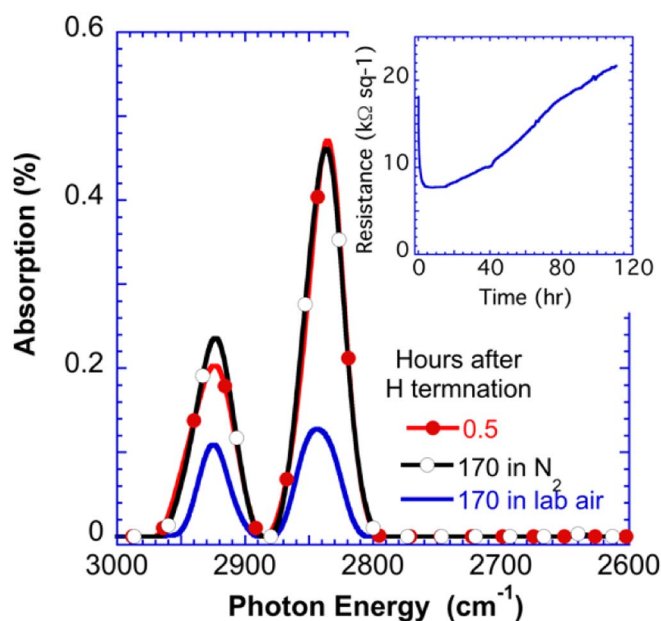


Fig. 17. C–H absorption spectra of two diamond powder H-terminated samples not activated. One is kept in dry  $\text{N}_2$  and the other in laboratory air. The insert shows the resistance of a (100) single crystal H-terminated diamond in laboratory air as a function of time.

$\text{NaHCO}_3$  solution to remove the  $\text{NO}_3^-$  and  $\text{NO}_2^-$  into the wash water. FTIR of the washed powder showed > 90% of the  $\text{NO}_3^-$  was removed by washing. The powder was allowed to settle out of the wash water over several hours and 0.1 ml of the wash solution was then diluted 9:1 with DI water and characterized by commercial chemical color kits obtained for  $\text{NO}_3^-$  and  $\text{NO}_2^-$ . These kits are commonly sold in aquarium and pet supply stores. Some kits require a pH adjustment with HCl to compensate for the  $\text{NaHCO}_3$ . The kits work by reacting  $\text{NO}_2^-$  with an amine to form a colored dye. For  $\text{NO}_3^-$  the first step is to reduce the  $\text{NO}_3^-$  ion to  $\text{NO}_2^-$  and the resulting  $\text{NO}_2^-$  is detected as before [39]. The kits have color charts, but using a simple spectrometer and calibration solutions of  $\text{NaNO}_3$  and  $\text{NaNO}_2$  a two-digit concentration of  $\text{NO}_3^-$  was obtained. The remainder of the wash solution was analyzed by ESMS. Typical ESMS mass spectrometer data of the wash solution is shown in Fig. 18. Our ESMS cannot measure the concentration of  $\text{NO}_2^-$ , but both the wet chemistry and ESMS agreed to within 30% for the concentration of  $\text{NO}_3^-$ . The chemical kits found no evidence of  $\text{NO}_2^-$  and set a lower surface concentration limit of  $< 10^{12}\text{ cm}^{-2}$ , at least 60 times less than the measured surface concentration of  $\text{NO}_3^-$ . The surface area of the diamond powder was determined to be  $47.3\text{ cm}^2\text{ mg}^{-1}$  by a (Brunauer, Emmett and Teller) BET process using  $\text{N}_2$  [41]. From the diamond powder surface area and the  $\text{NO}_3^-$  concentration the surface concentration of  $\text{NO}_3^-$  was calculated to be  $8.2 \times 10^{13}\text{ NO}_3^- \text{ cm}^{-2}$  by the kits and  $6.2 \times 10^{13}\text{ NO}_3^- \text{ cm}^{-2}$  by ESMS, which is within the same range as the measured carrier densities,  $3 \times 10^{13}$  to  $9 \times 10^{13}\text{ cm}^{-2}$ , made on single crystal diamonds [19].

## 3. Discussion

### 3.1. Experimental data interpretation

In all these experiments, no indication of  $\text{NO}_2^-$  has been found, only  $\text{NO}_3^-$ . It is known that  $\text{NO}_2$  will react with the matrix material, KBr, used for FTIR measurements to form  $\text{NO}_3^-$  salts [42].  $\text{NO}_3^-$  is seen in FTIR measurements of just KBr exposed to  $\text{NO}_2$  gas as discussed in the supplemental material. It is possible that the  $\text{NO}_3^-$  absorption is the result of residual  $\text{NO}_2$  gas after activation reacting with the KBr matrix. To address this possibility, FTIR measurements were made from the

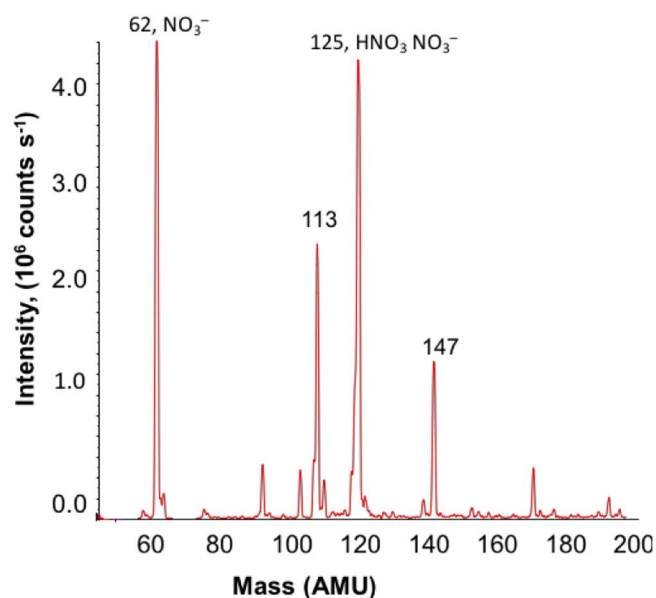


Fig. 18. Electrospray mass spectrometry (ESMS) data of water used to wash  $\text{NO}_2$ -activated diamond powder.

same H-terminated activated diamond powder 5 min and > 3 days after activation. The  $\text{NO}_3^-$  absorption measurements at  $1380\text{ cm}^{-1}$  were identical to within experimental error, Fig. 12, making it unlikely that residual  $\text{NO}_2$  gas is responsible for the  $\text{NO}_3^-$  absorption.

A second possibility is  $\text{NO}_2^-$  on the diamond surface might react with the KBr to form a  $\text{NO}_3^-$  salt. This possibility is also unlikely since the wet chemistry experiments have detected  $\text{NO}_3^-$ , but no  $\text{NO}_2^-$ . It seems that the most likely model is that  $\text{NO}_3^-$  formed on the diamond.

### 3.2. Modeling reactions to form $\text{NO}_3^-$

Two mechanisms are occurring during activation with  $\text{NO}_2$ . One where  $\text{NO}_2$  reacts to form  $\text{NO}_3^-$  and a second reaction where the C–H optical absorption between  $2800$  and  $2980\text{ cm}^{-1}$  is suppressed, presumably by  $\text{NO}_2$  reacting with the H atoms.  $\text{NO}_2$  is a radical with an unpaired electron that forms a dimer  $\text{N}_2\text{O}_4$ . At room temperature and pressure, the equilibrium partial pressures of  $\text{NO}_2$  and  $\text{N}_2\text{O}_4$  are about equal [43]. The first reaction is likely the result of electrons from the diamond onto  $\text{N}_2\text{O}_4$ .



Once  $\text{NO}_3^-$  is formed, the positive holes are stable near the diamond surface and the diamond can become conductive. A second reaction that can remove H from the diamond surface is;



Such reactions have been reported but usually occur for H atoms on carbon atoms double-bonded to another carbon atom [44]. The reaction that removes H saturates in minutes as indicated by optical absorption of C–H for different times of activation. The H–C absorption is reduced

but never completely removed. Additional  $\text{NO}_2$  exposure for 54 h, Fig. 16, shows that the optical absorption of C–H remains. At present the reactions of  $\text{NO}_2$  with the H surface of diamond are poorly understood and this reaction could be as important as the formation of  $\text{NO}_3^-$  to diamond's surface conduction.

The  $\text{NO}_3^-$  has several optical absorptions peaks [34,35]. Two are unresolvable in-plane vibrational modes near  $1380\text{ cm}^{-1}$ , which occur at the same wavenumber if the molecule is planar.  $\text{NO}_3^-$  has an additional out-of-plane vibration at  $\sim 830\text{ cm}^{-1}$ , which is either not observed or only appears as a very weak absorption peak. This mode does appear when the diamond powder is replaced with  $\text{NaNO}_3$  or when KBr is exposed to  $\text{NO}_2$  and forms  $\text{NO}_3^-$  as shown in the supplemental material. It is speculated that the out of plane vibration is damped by the one-sided electrostatic force between the  $\text{NO}_3^-$  and the positive charge in the diamond.

## 4. Conclusion

Several groups report [5,8,14,16,17,19] that  $\text{NO}_2$ -activation generates an initially low resistance that increases with time. It has been proposed that the resistance increases as the  $\text{NO}_2$  evaporates. However, using infrared absorption measurements, we observe no  $\text{NO}_2$  or  $\text{NO}_2^-$  on the diamond surface, but instead  $\text{NO}_3^-$ . The resistance and  $\text{NO}_3^-$  and H concentrations on the surface remained constant with time while kept in dry  $\text{N}_2$ . When exposed to laboratory air, the resistance increases and both  $\text{NO}_3^-$  and H concentrations decrease. Some chemical reaction with components in air is modifying the diamond surface and increasing its resistance. Efforts are ongoing to implement a method to isolate the conductive, activated surface from atmospheric contamination.

This report uses FTIR and chemical analysis results on powdered diamond, 0 to  $0.25\text{ }\mu\text{m}$ , implying the same chemistries are occurring on, > 3 mm on a side, (100) single-crystal diamonds. Single crystals have a well-defined crystal plane, (100) in this work, while the diamond powder has a stochastic distribution of crystal planes as indicated by the C–H absorption shown in Fig. 10. Single crystal diamonds become conductive when exposed to  $\text{NO}_2$  independent of the crystal planes, (100), (110) and (111), [12]. Both the powder and single crystal diamonds exhibit a significant decrease in resistance when activated in  $\text{NO}_2$ . It does not appear unreasonable to assume that H-termination and activation chemistries are the same for powder and single crystal diamonds.

Three disparate measurements of nitrogen surface concentration as measured by XPS on single crystal diamond, Fig. 2, by ESMS on diamond powder, Fig. 18, and by an analytical wet chemistry (aquarium) kit, all agree to within a factor of 3. Additionally, these measurements of diamond powder and single crystal diamond agree within a factor of 3 with Van der Paw-Hall measurements of carrier density (holes) of activated single crystal diamonds (Table 1).

An exact correspondence between the surface  $\text{NO}_3^-$  and the calculated hole densities is unlikely. The BET surface area assessment of powder is typically  $\pm 10\%$  [41]. The variation in hydrogen density on varied crystal planes present in the powder [12] implies a possible variation of  $\text{NO}_3^-$  of  $\pm 17\%$ . Analytical chemistry and ESMS are represented to be accurate within  $\pm 10\%$ , giving a total accuracy of  $\pm 22\%$  with respect to the single crystal values. Variation of the N

Table 1  
Measurements of diamond surface concentrations correlate with carrier density.

	Method	Carrier density ( $\text{cm}^{-2}$ )	$\text{NO}_3^-$ ( $\text{cm}^{-2}$ )	N ( $\text{cm}^{-2}$ )	$\text{NO}_2^-$ ( $\text{cm}^{-2}$ )
Single crystal	Van der Paw-Hall	$6 \pm 3 \times 10^{13}$			
	XPS			$1.5 \times 10^{14}$	
Diamond powder	ESMS		$6.2 \pm 1.4 \times 10^{13}$		
	Analytical chemistry		$8.2 \pm 1.8 \times 10^{13}$		$< 1 \times 10^{12}$

concentration determined by XPS is from the inconsistency of the measured and EAL of C1s electrons, (0.58–3 nm) [47]. Tanuma et al. [21] reported a 70% RMS variation in diamond's ELA where most other elements have variations of 10 to 20%. So, no estimate of the accuracy of the XPS measured nitrogen concentration is shown. The drift mobility, which is preferable to Hall mobility to obtain the hole density, can differ from the Hall mobility by several tens of percent [45].

One of the properties of NO<sub>2</sub>-activation is the removal of H from the diamond surface. How that affects the surface conduction is unknown. Other compounds that increase the surface conductance, O<sub>3</sub> [14], (NH<sub>4</sub>)<sub>3</sub>Cs(NO<sub>3</sub>)<sub>6</sub> [19], V<sub>2</sub>O<sub>5</sub> [10,46], MoO<sub>3</sub> [9], WO<sub>3</sub> [48] ReO<sub>3</sub> [48] are all oxidizers as well as electron acceptors. To our knowledge, the surface chemistry of these compounds has not been investigated.

## Acknowledgement

The authors are grateful to Bradley Duncan and Shireen Warnock for helpful scientific and technical discussions, Donna Lennon for XPS characterization, Alla Ostrinskaya and, Sandra Deneault for ESMS, and for the expert technical assistance of Chelesea Peragallo, Michael Marchant, and Peter Murphy. **Distribution statement A**

Approved for public release: distribution unlimited. This material is based upon work supported by the Assistant Secretary of Defense for Research and Engineering under Air Force Contract No. FA8721-05-C-0002 and/or FA8702-15-D-0001. Any opinions, findings, conclusions or recommendations expressed in this material are those of the author(s) and do not necessarily reflect the views of the Assistant Secretary of Defense for Research and Engineering.

## Appendix A. Supplementary data

Supplementary data to this article can be found online at <https://doi.org/10.1016/j.diamond.2018.03.002>.

## References

- [1] M.I. Landstrass, K.V. Ravi, Resistivity of chemical vapor deposited diamond films, *Appl. Phys. Lett.* 55 (1989) 975–977.
- [2] R.S. Gi, T. Mizumasa, Y. Akiba, Y. Hirose, Formation mechanism of p-type surface conductive layer on deposited diamond films, *Jpn. J. Appl. Phys.* 34 (1995) 5550–5555.
- [3] P. Strobel, M. Riedel, J. Ristein, L. Ley, Surface transfer doping of diamond, *Nature* 430 (2004) 439–431.
- [4] H. Kawarada, T. Yamada, D. Xu, H. Tsuboi, T. Saito, A. Hiraiwa, Wide temperature (10 K–700 K) and high voltage (~1000 V) operation of CH diamond MOSFETs for power electronics application, *Electron Device Meeting (IEDM), IEEE Int.* 11 (2) (2014) 1–4.
- [5] K. Hirama, H. Sato, Y. Harada, H. Yamamoto, M. Kasu, Diamond field-effect transistors with 1.3 A/mm drain current density by Al<sub>2</sub>O<sub>3</sub> passivation layer, *Jpn. J. Appl. Phys.* 51 (2012) 090112.
- [6] M. Syamsul, Y. Kitabayashi, D. Matsumura, T. Saito, Y. Shintani, H. Kawarada, High voltage breakdown (1.8 kV) of hydrogenated black diamond field effect transistor, *Appl. Phys. Lett.* 109 (2016) 203504.
- [7] S.A.O. Russell, S. Sharabi, A. Tallaire, D.A.J. Moran, RF operation of hydrogen-terminated diamond field effect transistors: a comparative study, *IEEE Trans. Electron Devices* 62 (3) (2015) 751–756.
- [8] M. Kasu, Diamond field-effect transistors for RF power electronics: novel NO<sub>2</sub> hole doping and low temperature deposited Al<sub>2</sub>O<sub>3</sub> passivation, *Jpn. J. Appl. Phys.* 56 (2017) 01AA01.
- [9] S.A.O. Russell, L. Cao, D. Qi, A. Tallaire, K.G. Crawford, A.T.S. Wee, D.A.J. Moran, Surface transfer doping of diamond by MoO<sub>3</sub>: a combined spectroscopic and Hall measurement study, *Appl. Phys. Lett.* 103 (2013) 202112.
- [10] A. Vardi, M. Tordjman, J.A. del Alamo, R. Kalish, A diamond:H/MoO<sub>3</sub> MOSFET, *IEEE Electron Device Lett.* 35 (12) (2014) 1320–1322.
- [11] C. Verona, W. Ciccognani, S. Colangeli, E. Limiti, M. Marinelli, G. Verona-Rinati, D. Cannatà, M. Benetti, F. Di Pietranton, V<sub>2</sub>O<sub>5</sub> MISFETs on H-terminated diamond, *IEEE Trans. Electron Devices* 63 (2016) 4647–4653.
- [12] H. Sato, M. Kasu, Maximum hole concentration for hydrogen-terminated diamond surfaces with various surface orientations obtained by exposure to highly concentrated NO<sub>2</sub>, *Diam. Relat. Mater.* 31 (2013) 47–49.
- [13] R. Sung Gi, T. Ishikawa, S. Tanaka, T. Kimura, Y. Akiba, M. Iida, Possibility of realizing a gas sensor using surface conductive layer on diamond films, *Jpn. J. Appl. Phys.* 36 (4A) (1997) 2057–2060.
- [14] H. Sato, M. Kasu, Electronic properties of H-terminated diamond during NO<sub>2</sub> and O<sub>3</sub> adsorption and desorption, *Diam. Relat. Mater.* 24 (2012) 99–103.
- [15] Massachusetts, Air Quality Report, Department of Environmental Protection, Bureau of Air and Waste, Division of Air and Climate Programs, 37 Air Assessment Branch, Wall Experiment Station, Shattuck Street, Lawrence, Massachusetts, 2016, p. 01843.
- [16] Y. Takagi, K. Shiraiishi, M. Kasu, H. Sato, Mechanism of hole doping into hydrogen terminated diamond by the adsorption of inorganic molecule, *Surf. Sci.* 609 (2013) 203–206.
- [17] P. Rivero, W. Shelton, V. Meunier, Surface properties of hydrogenated diamond in the presence of adsorbates: a hybrid functional DFT study, *Carbon* 110 (2016) 469–479.
- [18] M. Kubovic, M. Kasu, H. Kageshima, F. Maeda, Electronic and surface properties of H-terminated diamond surface affected by NO<sub>2</sub> gas, *Diam. Relat. Mater.* 19 (2010) 889–893.
- [19] T. Wade, M.W. Geis, T.H. Fedynshyn, S.A. Vitale, J.O. Varghese, D.M. Lennon, T.A. Grotjohn, R.J. Nemanich, M.A. Hollis, Effect of surface roughness and H-termination chemistry on diamond's semiconducting surface conductance, *Diam. Relat. Mater.* 76 (2017) 79–85.
- [20] V.M. Bermudez, Study of oxygen chemisorption on the GaN(0001)-(1 $\bar{1}$ –1) surface, *J. Appl. Phys.* 80 (1996) 1190–1200, <http://dx.doi.org/10.1063/1.362924>.
- [21] S. Tanuma, C.J. Powell, D.R. Penn, Calculations of electron inelastic mean free paths. IX. Data for 41 elemental solids over the 50 to 30 keV range, *Surf. Interface Anal.* 43 (2011) 689–713.
- [22] Y. Yang, F.A. Koeck, M. Dutta, X. Wang, S. Chowdhury, R.J. Nemanich, Al<sub>2</sub>O<sub>3</sub> dielectric layers on H-terminated diamond: controlling surface conductivity, *J. Appl. Phys.* 122 (2017) 155304, <http://dx.doi.org/10.1063/1.4985808>.
- [23] J.F. Moulder, W.F. Stickle, P.E. Sobol, K.D. Bomben, J. Chastaiun (Ed.), *Handbook of X-ray Photoelectron Spectroscopy*, Perkin-Elmer Corporation, Eden Prairie, MN USA, 1992.
- [24] [https://www.youtube.com/watch?v=ITAHqg\\_Q\\_5I](https://www.youtube.com/watch?v=ITAHqg_Q_5I).
- [25] M. Pierza, J. Sawatzki, Method and Device for Correcting a Spectrum, US Patent 7,359,815 B2.
- [26] Y. Maréchal, The molecular structure of liquid water delivered by absorption spectroscopy in the whole IR region completed with thermodynamics data, *J. Mol. Struct.* 1004 (2011) 146–155.
- [27] *Water Absorption Spectrum*, [http://www1.lsbu.ac.uk/water/water\\_vibrational\\_spectrum.html](http://www1.lsbu.ac.uk/water/water_vibrational_spectrum.html).
- [28] B.D. Thorns, J.E. Butler, HREELS scattering mechanism from diamond surfaces, *Phys. Rev. B* 50 (23) (1994) 17450–17455.
- [29] F. Maier, M. Riedel, B. Mantel, J. Ristein, L. Ley, Origin of surface conductivity in diamond, *Phys. Rev. Lett.* 85 (16) (2000) 3472–3475.
- [30] M. McGonigal, J.N. Russell Jr., P.E. Pehrsson, H.G. Maguire, J.E. Butler, Multiple internal reflection infrared spectroscopy of hydrogen adsorbed on diamond (110), *J. Appl. Phys.* 77 (8) (1995) 4049–4053.
- [31] B.F. Mantel, M. Stammler, J. Ristein, L. Ley, Fourier transform infrared spectroscopy of CMH vibrational modes on a diamond (111) surface, *Diam. Relat. Mater.* 9 (2000) 1032–1035.
- [32] R.P. Chin, J.Y. Huang, T.J. Chuang, H. Seki, Y.R. Shen, Interactions of hydrogen and methyl radicals with diamond C.111 studied by sum-frequency vibrational spectroscopy, *Phys. Rev. B* 54 (11) (1996) 8243–8251.
- [33] G.R. Brandes, A.P. Mills Jr., Work function and affinity changes associated with the structure of hydrogen-terminated diamond (100) surfaces, *Phys. Rev. B* 58 (8) (1998) 4952–4962.
- [34] L. Harris, G.W. King, The infrared absorption spectra of nitrogen dioxide and tetroxide, *J. Chem. Phys.* 2 (2) (1934) 51–57.
- [35] M. Reichenbacher, J. Popp (Eds.), *Vibrational Spectroscopy in Challenges in Molecular Structure Determination*, Ch2, Springer-Verlag, Berlin Heidelberg, 2012, p. 79.
- [36] M.H. Brooker, D.E. Irish, Infrared and Raman spectral studies of KNO<sub>2</sub>-KNO<sub>3</sub> solutions, *Can. J. Chem.* 46 (1968) 229–233.
- [37] E. Silberman, H.W. Morgan, Infrared spectra of the nitrite ion in solid solution, *Spectrochim. Acta* 23A (1967) 2855–2857.
- [38] M. Kubovic, M. Kasu, H. Kageshima, Sorption properties of NO<sub>2</sub> gas and its strong influence on hole concentration of H-terminated diamond surfaces, *Appl. Phys. Lett.* 96 (2010) 052101.
- [39] C. J. Patton, J. R. Kryskalla, Analytical Properties of Some Commercially Available Nitrate Reductase Enzymes Evaluated as Replacements for Cadmium in Automated, Semiautomated, and Manual Colorimetric Methods for Determination of Nitrate Plus Nitrite in Water, U.S. Geological Survey Office of Water Quality, National Water Quality Laboratory, (Scientific Investigations Report 2013-5033).
- [40] C.S. Ho, C.W.K. Lam, M.H.M. Chan, R.C.K. Cheung, L.K. Law, L.C.W. Lit, K.F. Ng, M.W.M. Suen, H.L. Tai, Electro spray ionization mass spectrometry: principles and clinical applications, *Clin. Biochem. Rev.* 24 (2003) 3–12.
- [41] S. Brunauer, P.H. Emmett, E. Teller, Adsorption of gases in multimolecular layers, *J. Am. Chem. Soc.* 60 (2) (1938) 309–319.
- [42] B.J. Finlayson-Pitts, S.N. Johnson, The reaction of NO<sub>2</sub> with NaBr: possible source of BrNO in polluted marine atmospheres, *Atmos. Environ.* 22 (6) (1988) 1107–1112.
- [43] W.F. Giauque, J.D. Kemp, The entropies of nitrogen tetroxide and nitrogen dioxide. The heat capacity from 15°K to the boiling point. The heat of vaporization and vapor pressure. The Equilibria N<sub>2</sub>O<sub>4</sub> = 2NO<sub>2</sub> = 2NO + O<sub>2</sub>, *J. Chem. Phys.* 6 (1938) 40–52.
- [44] D.H. Giamalva, G.B. Kenion, D.F. Church, W.A. Pryor, Rates and mechanisms of reaction of nitrogen dioxide with alkenes in solution, *J. Am. Chem. Soc.* 109 (1987) 7059–7063.

- [45] L. Reggiani, D. Waechter, S. Zukotynski, Hall-coefficient factor and inverse valence-band parameters of holes in natural diamond, *Phys. Rev. B* 28 (1983) 3550–3554.
- [46] K.G. Crawford, L. Cao, D. Qi, A. Tallaire, E. Limiti, C. Verona, A.T.S. Wee, D.A.J. Moran, Enhanced surface transfer doping of diamond by V2O5 with improved thermal stability, *Appl. Phys. Lett.* 108 (2016) 042103.
- [47] S. Kono, T. Saitou, H. Kawata, T. Goto, Y. Kakefuda, T. Komeda, Characteristic energy band values and electron attenuation length of a chemical-vapor-deposition diamond (001) $2 \times 1$  surface, *Surf. Sci.* 603 (2009) 860–866.
- [48] M. Tordjman, K. Weinfeld, R. Kalish, Boosting surface charge-transfer doping efficiency and robustness of diamond with WO<sub>3</sub> and ReO<sub>3</sub>, *Appl. Phys. Lett.* 111 (2017) 111601.